Temperature Dependence of the Backbone Dynamics of Ribonuclease A in the Ground State and Bound to the Inhibitor 5′-Phosphothymidine (3′-5′)Pyrophosphate Adenosine 3′-Phosphate†

Evgenii L. Kovrigin, Roger Cole, and J. Patrick Loria*

Department of Chemistry, Yale University, P.O. Box 208107, New Haven, Connecticut 06520

Received January 9, 2003; Revised Manuscript Received March 23, 2003

ABSTRACT: The interaction of the dinucleotide inhibitor 5′-phosphothymidine(3′,5′)pyrophosphate adenosine 3′-phosphate (pTppAp) with bovine pancreatic ribonuclease A (RNase A) was characterized by calorimetry and solution NMR spectroscopy. Calorimetric data show that binding of pTppAp to RNase A is exothermic ($\Delta H = -60.1 \pm 4.1$ kJ/mol) with a dissociation constant of 16 nM at 298 K. At this temperature, the binding results in an entropy loss ($T\Delta S = -16.8 \pm 7.3$ kJ/mol) that is more favorable than that with the product analogue, 2′-CMP ($T\Delta S = -31.3 \pm 0.9$ kJ/mol). Temperature-dependent calorimetric experiments give a ΔC_p for ligand binding of -230 ± 100 J/mol K. Binding of pTppAp results in noticeable effects on the backbone amide chemical shifts and dynamics. Amide backbone ^{15}N NMR spin-relaxation studies were performed on both apo RNase A and RNase A/pTppAp as a function of temperature. At each temperature, the model-free-determined order parameters, S^2, were significantly higher for RNase A/pTppAp than for the apo enzyme indicating a decrease in the conformational entropy of the protein upon ligand binding. Furthermore, the magnitude of this difference varies along the amino acid sequence specifically locating the entropic changes. The temperature dependence of S^2 at each residue enabled assessment of the local heat capacity changes (ΔC_p) from ligand binding. In an overall, average sense, ΔC_p for the protein backbone, determined from the NMR dynamics measurements, did not differ between apo RNase A and RNase A/pTppAp indicating that backbone dynamics contribute little to ΔC_p for protein−ligand interactions in this system. However, residue-by-residue comparison of the temperature-dependent change in entropy (ΔS_B) between free and bound forms reveals nonzero contributions to ΔC_p at individual sites. The balance of positive and negative changes reveals a redistribution of energetics upon binding. Furthermore, experiment and semiempirical estimates suggest that a large negative ΔC_p should accompany binding of pTppAp, and we conclude that this contribution must arise from factors other than amide backbone dynamics.

NMR studies of the temperature dependence of enzyme dynamics can provide access to site specific kinetic and thermodynamic information while aiding to define the potential energy surface of the motion. The study of enzymes in conformational states resembling an activated complex or nonground state configuration is facilitated through the use of ligands designed to mimic a particular reaction path intermediate. This practice is commonly employed in crystallographic or NMR structural analysis to aid in understanding enzyme mechanisms but has not been widely exploited to assess the role of protein dynamics at positions along the reaction coordinate. Here, we address this issue through a comparison of the temperature-dependent backbone amide order parameters derived from solution NMR for the enzyme ribonuclease A in the apo form and in a complex with the nanomolar inhibitor, pTppAp.[1]

Bovine pancreatic RNase A catalyzes the cleavage of single-stranded RNA. The enzymatic reaction occurs in a distributive fashion in which RNase A binds the RNA polymer, cleaves the nucleic acid chain, and releases the products into solution (*1*). RNase A is secreted in large amounts by the pancreas and is thought to function primarily as a digestive enzyme. More recently, the ribonuclease family of enzymes has received increased attention due to the therapeutic benefits elicited by their cytotoxic and angiogenic properties (*2*−*4*). These unanticipated effects present encouraging new routes for the treatment of disease.

RNase A has been a model system for the study of protein folding (*5*), chemistry (*6*, *7*), and structure (*8*) as well as mechanistic enzymology (*9*, *10*, and references therein). The overall shape of RNase A approximates an ellipse. The active

† J.P.L. acknowledges support from the Camille and Henry Dreyfus New Faculty Fellowship and a grant from the Hellman Family Foundation. E.L.K. acknowledges a Rudolph Anderson Postdoctoral Fellowship, and R.C. thanks the NSF for a graduate research fellowship.

* To whom correspondence should be addressed. Tel: 203-436-4847. Fax: 203-432-6144. E-mail: patrick.loria@yale.edu.

[1] Abbreviations: 2′-CMP, 2′-cytidine monophosphate; pTppAp, 5′-phosphothymidine(3′,5′)pyrophosphate adenosine 3′-phosphate; pdUppAp, 5′-phosphodeoxyuridine(3′,5′)pyrophosphate adenosine 3′-phosphate; R_1, ^{15}N longitudinal spin-relaxation rate; R_2, ^{15}N transverse spin-relaxation rate; η_{xy}, transverse ^{1}H−^{15}N dipole/^{15}N CSA interference rate; DCC, dicyclohexylcarbodiimide; apo RNase A, RNase A in the absence of ligand; RNase A/pTppAp, RNase A bound to the inhibitor pTppAp.

10.1021/bi034027h CCC: $25.00
Published on Web 04/15/2003

Scheme 1: (A) Chemical Structure of pTppAp and (B) Ribbon Diagram of Bovine Pancreatic Ribonuclease with 2° Structure Elements Identified

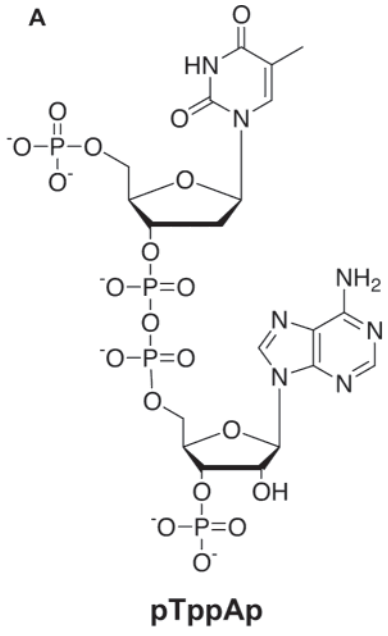

site resides in a cleft, the bottom of which is primarily comprised of three long antiparallel β-sheets. The enzyme is also composed of two short β-strands, three α-helices, and six loop or turn regions (Scheme 1). Additional structural integrity is provided by eight cysteine residues, all involved in disulfide bonds resulting in a highly stable enzyme. RNase A is a small (13.7 kDa) enzyme that cleaves single-stranded RNA specifically on the 3′-side of pyrimidine residues. The enzyme is a very efficient catalyst ($k_{cat}/k_{uncat} \sim 10^{11}$) (*11*); in addition, substrate binding occurs with a bimolecular rate constant on the order of 10^7-10^8 M^{-1} s^{-1} (*11*, *12*) and product release at a rate of $\sim 10^3$ s^{-1} (*13*). During the catalytic cycle, RNase A displays significant flexibility and undergoes several conformational changes (*14*) and we have previously uncovered evidence of a functional role for these dynamics (*15*).

Enzymes, in general, represent ideal systems for investigating the role of dynamics in macromolecular function. By necessity, enzymes alter their conformation as the catalytic reaction progresses from substrate to transition state to product state (*16*). Recent studies have additionally acknowledged the potential role of ground state motions in catalytic processes (*17*, *18*). Efforts to elucidate the role of fast time scale (picosecond to nanosecond; ps−ns) dynamics in enzyme function are numerous and cover a range of experimental and theoretical approaches. Among these, spectroscopic (*19*−*24*) and X-ray crystallographic (*25*, *26*) investigations of enzyme dynamics have been carried out. Other studies such as hydrogen/deuterium exchange experiments have linked protein flexibility with the degree of hydrogen tunneling in alcohol dehydrogenase (*27*). Furthermore, computational arguments (*17*, *18*, *28*−*30*) for the role of dynamics in enzyme function have been reported. Experimental work has demonstrated correlation of both specificity (*31*) and entantioselectivity (*32*) with enzyme dynamics. In addition to the aforementioned ps−ns dynamics, motions on a slower time scale (microsecond to millisecond; μs−ms) that can limit substrate binding, product release, and catalytic steps have been characterized by NMR (*15*, *23*, *33*−*36*). The close link between function and flexibility implied by these studies warrants further investigation into the details of the energy landscape and mechanistic impact of enzyme motion.

Temperature can have a profound affect on macromolecular function via changes in structure and dynamics. For example, RNase A ceases to bind ligand at 200 K (*9*). Variable temperature (98−300 K) X-ray crystallographic studies of ribonuclease A indicate a modest linear expansion in protein volume with temperature (*26*), primarily due to movement of solvent-exposed loop regions. Interestingly, the concurrent change in the Debye−Waller factors and broadening of their distribution suggests an increase in anharmonic protein motions (*26*). A complementary view of protein dynamics can be obtained from NMR spectroscopy. The amplitudes of intramolecular bond vector fluctuations (the order parameter, S^2) have been characterized via solution NMR spin-relaxation studies, for example, in characterization of the thermodynamics of Ca^{2+} binding and cooperativity in the protein Calbindin D_{9K} (*37*). In other works, a relationship between S^2 and configurational entropy has been established (*38*, *39*) and subsequently used to dissect the contributions of conformational entropy to protein folding (*39*) and DNA binding (*40*). Additionally, the temperature dependence of S^2 was used to describe the protein backbone contribution to the conformational heat capacity in the folded and unfolded state for an SH3 domain, for staphylococcal nuclease and for protein G (*41*, *42*). In a significant achievement, Wand and co-workers characterized side chain and backbone dynamics of a calmodulin−peptide complex at 13 temperatures (*43*, *44*). Their work indicates that protein dynamics are remarkably heterogeneous and provides additional insight into the factors governing protein stability. NMR studies with the enzyme ribonuclease HI established that the mobility of loops and termini exhibits substantial temperature dependence while secondary structure dynamics were not as temperature sensitive (*45*). In regard to these studies, a fundamental question of enzymology emerges; how do the fluctuations of an enzyme respond to the presence of ligands, especially those ligands that structurally mimic positions along the reaction coordinate? To address this issue here, we have characterized the temperature dependence of

ps−ns backbone dynamics in RNase A in the ground state and for RNase A bound to the nanomolar inhibitor pTppAp through the use of ^{15}N spin-relaxation measurements. These studies also provide further insight into the response of millisecond motion to ligand binding.

METHODS AND THEORY

Protein Expression and Purification. Escherichia coli strain BL21(DE3) was from Novagen (Madison, WI). All buffers and salts were from Sigma Chemical (St. Louis, MO). Deuterated buffers were from Cambridge Isotope Laboratories. The plasmid, pBXR, encoding for bovine pancreatic ribonuclease A, was a generous gift of Professor Ronald T. Raines (University of Wisconsin−Madison). Isotopically ^{15}N-labeled RNase A was expressed and purified according to published protocols (*46*) with the modification that the final growth be performed in M9 media containing 1 g/L ^{15}N NH_4Cl and glucose and supplemented with vitamins and trace metals. Ribonuclease was purified and refolded by the method outlined by Raines and co-workers (*46*). The purity of the final RNase A product was determined to be >98% by sodium dodecyl sulfate polyacrylamide gel electrophoresis and mass spectrometry. For NMR experiments, RNase A was in a solution containing 5 mM deuterated MES, pH 6.4, and 10 mM NaCl. The concentration of RNase A was determined using an extinction coefficient, $\epsilon_{278} = 9800\ M^{-1}\ cm^{-1}$ (*47*).

Inhibitor Synthesis and Characterization. The inhibitor pTppAp (5′-phosphothymidine-3′-pyrophosphate adenosine-3′-phosphate) was synthesized in a fashion similar to published protocols (*48*, *49*). Briefly, a mixture of 2′,5′- and 3′,5′-adenosine diphosphate was converted to the corresponding morpholinium salts using a Dowex-50 cation exchange column. Treatment of the resulting mixture with DCC and morpholine furnished adenosine 2′,3′-cyclic phosphate 5′-phosphomorpholidate as its bis(4-morpholine-*N*,*N*′-dicyclohexylcarboxamidinium) salt. This material was dried via several evaporations from anhydrous pyridine. The phosphomorpholidate moiety was sufficiently activated to form the desired pyrophosphate bond upon treatment with the tri-*n*-butylammonium salt of thymidine-3′-phosphate in anhydrous pyridine at 40 °C. The 2′,3′-cyclic phosphate was then selectively cleaved to the corresponding 3′-phosphate by incubation with ribonuclease T2. The material was purified by anion exchange chromatography using a Resource Q column and linear gradient of triethylammonium bicarbonate (TEAB) that was eventually removed by lyophilization. The final 5′-phosphate group on the thymidine nucleotide was then introduced through the action of the enzyme T4-polynucleotide kinase. Pure pTppAp was isolated by ion exchange chromatography, again using the Resource Q column and TEAB gradient elution. The progress of all reactions was monitored by ^{31}P NMR. The final product was characterized by electrospray ionization-MS analysis, $^1H-^1H$ correlation spectroscopy (COSY), and $^1H-^{31}P$ HMQC NMR experiments. All spectroscopic data were fully consistent with the proposed structure. The concentration of pTppAp was determined by ^1H NMR in the following manner. ATP, at a concentration of 50 μM (determined using an extinction coefficient of 15 400 $M^{-1}\ cm^{-1}$), was placed in an NMR tube with a measured but unknown concentration of pTppAp (triethylammonium salt). A fully relaxed one-dimensional ^1H NMR spectrum (2000 transients) was acquired with a 25 s recycle delay (the R_1 of the relevant protons is ca. 1 s^{-1} (*50*)). The areas of the resonances corresponding to the adenine H2 protons of ATP and pTppAp and the thymidine H6 proton of pTppAp were determined (supplemental information). The ratio of pTppAp-to-ATP peak areas was used to determine the amount of pTppAp present in the original stock solution.

Inhibitor Binding. Binding of pTppAp and cytidine 2′-monophosphate (2′-CMP) to RNase A was determined using titration calorimetry. Ligand was titrated into a thermostated solution of RNase A in 20 mM MES, pH 6.4, using Microcal MCS and VP titration calorimeters. RNase A concentrations were 43.7 and 2.8 μM, respectively, for the 2′-CMP and pTppAp binding experiments. Cytidine monophosphate concentrations were determined using a molar extinction coefficient of 7600 $M^{-1}\ cm^{-1}$ (*47*), and pTppAp concentration was determined as described above. Binding of pTppAp to RNase A was quantitated by fitting the evolved heat to the following equation (*51*)

$$\Delta q = n[M]_T V_{cell} \Delta H_{app} \times \mathscr{R} = \Delta q_{app} - \Delta q_{dil} - \Delta q_{ns} \quad (1)$$

in which $\mathscr{R}$ is the root of

$$Y_i^2 - Y_i \times \left(1 + \frac{1}{nK_a[M]_T} + \frac{[L_i]_T}{n[M]_T}\right) + n[L_i]_T[M]_T = 0 \quad (2)$$

In eqs 1 and 2, Δq is the apparent heat change upon ligand binding, Δq_{dil} is the heat of dilution, Δq_{ns} is the heat due to nonspecific interactions, n is the number of binding sites, V_{cell} is the volume of the calorimetric cell, K_a is the association constant, M_T and L_T are the total macromolecule and ligand concentrations, respectively, and Y_i is the degree of saturation. Once K_a and $\Delta H°$ are known from calorimetry, $\Delta G°$ and $\Delta S°$ were calculated from

$$\Delta G° = -RT \ln K_a \quad (3)$$

$$\Delta S° = (\Delta H° - \Delta G°)/T \quad (4)$$

in which R is the gas constant and T is the absolute temperature.

The heat capacity change (ΔC_p) for pTppAp binding to RNase A was measured from temperature-dependent calorimetric enthalpy values and estimated by semiempirical methods based on the burial of polar and nonpolar surface area concomitant with the binding reaction (*52*, *53*). Precise values of enthalpies of pTppAp binding to RNase A at the three temperatures (280, 298, and 310 K) were determined in separate titration experiments. Aliquots of pTppAp were injected into the cell containing an excess amount of RNase A to ensure complete inhibitor binding. Experiments were carried out in triplicate at each temperature. Heats of pTppAp injections into the buffer without RNase A were subtracted, and results were averaged. The heat capacity change was determined by linear fitting of ΔH as a function of temperature. Surface area calculations were performed with the program Naccess (*54*). A probe radius of 1.4 Å was used for surface area calculations. For the binding reaction, RNase A + pTppAp ↔ RNase A/pTppAp, the changes in the polar

and nonpolar solvent accessible surface area (SAS) were determined from

$$\Delta SAS_{np} = SAS_{np}^{complex} - (SAS_{np}^{free\text{-}enzyme} + SAS_{np}^{free\text{-}ligand}) \quad (5)$$

$$\Delta SAS_{p} = SAS_{p}^{complex} - (SAS_{p}^{free\text{-}enzyme} + SAS_{p}^{free\text{-}ligand}) \quad (6)$$

where np and p indicate nonpolar and polar contributions to the SAS for the free and bound protein and ligand. The structure of the free ligand was determined using the Merck 94 force field as implemented in Spartan 5.1 (Wavefunction, Inc., Irvine, CA). The surface area calculation for apo RNase A was based upon the atomic coordinates from the crystal structure 7RSA (*55*). No three-dimensional structure for the RNase A/pTppAp complex exists. However, an X-ray crystal structure of RNase A bound to the related compound, p(dU)-ppAp, is available (*56*). The SAS calculation of the RNase A/pTppAp complex was determined by building the thymidine moiety of pTppAp onto the uridine group in the crystal structure of the RNase A/p(dU)ppAp complex (accession 1QHC) (*56*).

NMR Experiments. All protein NMR experiments were performed on a 600 μM ^{15}N-lableled RNase A sample using a four channel Varian Inova 600 MHz instrument and a *Z* gradient-equipped Varian HX probe. Typically, 22 μs ^{15}N 90° pulse widths were achievable with this probe. The experimental temperature was calibrated using a 100% methanol standard. Ambiguities in resonance assignments were resolved by recording a ^{15}N-nuclear Overhauser enhancement spectroscopy (NOESY)−HSQC at each temperature. NMR spin-relaxation experiments were performed at each temperature using published, gradient-selected, sensitivity-enhanced pulse sequences (*57*−*59*). The longitudinal (R_1) spin-relaxation rates were measured with T_1 delays of 2 (×3), 132, 272, 442, 632, 862 (×2), 1502, and 1802 ms. The transverse (R_2) relaxation rates were obtained with 1.0 ms spacing between ^{15}N 180° CPMG pulses at total relaxation delays of 2 (×2), 12, 36, 54, 78 (×2), 134, and 250 ms. For R_2 measurements, temperature-compensating ^{15}N 180° pulses were applied during the recycle delay and ^{15}N 180° pulse widths were lengthened to 76 μs to reduce sample heating (*60*). The heteronuclear cross-relaxation rate (NOE) was obtained by interleaving pulse sequences with and without proton saturation. Measurement of transverse cross-relaxation (η_{xy}) rates mediated by ^{15}N−CSA/dipolar interference was achieved as described previously with relaxation delays of 32, 53.4, 74.8, 96.1, and 106.7 ms (*61*, *62*). All relaxation spectra were acquired with the ^{1}H carrier set coincident with the water resonance and ^{15}N frequency set to 120 ppm; spectral widths were 12 000 and 1900 Hz in the t_2 and t_1 dimensions with 2048 and 128 complex points in each dimension, respectively. A recycle delay of 2.6 s was used in all (R_1, R_2, and η_{xy}) relaxation experiments. NMR data were processed with NMRPipe (*63*) and visualized with Sparky (*64*). Longitudinal and transverse relaxation rates were determined by fitting the peak heights (obtained from a 3 × 3 grid located at the peak maxima) to a single exponential decay by a nonlinear least squares routine using in-house written software and the program Curvefit provided by Professor Arthur G. Palmer (http://cpmcnet.columbia.edu/dept/gsas/biochem/labs/palmer/software.html). The heteronuclear NOE was determined from the ratio of peak heights for experiments with and without ^{1}H saturation pulses. The transverse cross-relaxation rate (η_{xy}) was determined from the ratio of peak intensities from experiments detecting S_y (I_{cross}) and $2I_zS_y$ (I_{auto}) coherences (*61*, *62*) where

$$I_{cross}/I_{auto} = \tanh(\eta_{xy}\tau) \quad (7)$$

in which τ is the experimental relaxation delay. Relaxation rates for overlapping peaks were determined using a separate Lorentz-to-Gauss resolution enhancement processing scheme (*58*).

Model-Free Analysis. Protein amide backbone dynamics were characterized by fitting NMR spin-relaxation rates to one of five semiempirical forms of the spectral density function using model-free analysis (*65*, *66*). The five models used to describe the spin-relaxation data are described according to their corresponding free parameters in eq 8 (*21*)

$$\begin{aligned}&\text{model 1, } S^2;\ \text{model 2, } S^2, \tau_e;\ \text{model 3, } S^2, R_{ex};\\ &\text{model 4, } S^2, \tau_e, R_{ex};\ \text{model 5, } S_f^2, S^2, \tau_e\end{aligned} \quad (8)$$

in which τ_e is the internal correlation time; S^2 is the generalized order parameter; S_f^2 is the order parameter for fast motion, with typical correlation time <10 ps; and R_{ex} is the additional line broadening due to conformational exchange and depends on the equilibrium site populations, the chemical shift differences, and the rate of exchange between conformers. Fitting of motional parameters to the spin-relaxation data was performed using the selection protocol described for the program FAST-Modelfree (*67*) interfaced with Model-Free 4.01 (*21*, *68*). Model selection was based on the statistical testing protocol described previously by Mandel et al. (*21*). The rotational diffusion tensor for RNase A was estimated from R_2/R_1 ratios and the program R2R1_diffusion using the X-ray crystal coordinates, (7RSA (*55*)) and the program pdbinertia (provided by Professor Arthur G. Palmer). The criteria for inclusion of residues in the diffusion tensor estimate relied on the method of Tjandra et al. (*69*) and by additional exclusion of residues with η_{xy}/R_2 greater than one standard deviation from the mean value. During the model-free analysis, N−H bond lengths were assumed to be 1.02 Å and the ^{15}N chemical shift anisotropy was estimated as −160 ppm (*70*, *71*). Some studies have indicated the existence of variability in ^{15}N CSA values (*72*); however, these experiments were not performed with RNase A, and therefore, standard values were used in this work. For each model, 1000 randomly distributed data sets were generated. Models were selected by comparing the sum-squared error of the optimal fit with the 0.05 critical value of the distribution. In cases where *F* statistics were applicable, comparisons were made with the 0.20 critical value of the distribution. During the model selection process, the diffusion tensor parameters were kept fixed. Once models had been assigned to each spin, the diffusion tensor and model parameters were optimized simultaneously. The process of model selection was then repeated until the optimized tensor parameters and S^2 did not differ significantly from those from the previous round of model selection. Spin-relaxation data at all temperatures were analyzed independently to obtain values for $D_\parallel/D_\perp$, ϕ, and θ. The resulting values at each individual temperature varied over the full temperature range by 3, 4, and 0.4%, respectively. Therefore, after model

selection and parameter optimization, all motional parameters were optimized a final time by rerunning Modelfree 4.01 with fixed average values of $D_{\parallel}/D_{\perp}$, ϕ, and θ.

The order parameter, S^2, obtained from model-free analysis, can be expressed in terms of a configurational entropy value for the angular fluctuation of the individual N−H bond vector according to (*38*, *39*, *73*)

$$S_B = k_B \ln[\pi(3 - (1 + 8S)^{1/2})] \quad (9)$$

in which S_B is the entropy and k_B is Boltzmann's constant. The temperature dependence of S_B can be further expressed in terms of a local heat capacity

$$C_p = \frac{dS_B}{d \ln (T)} \quad (10)$$

for each N−H bond (*42*).

Alternatively, if the N−H bond vector motion is modeled as angular fluctuations within an axially symmetric parabolic potential, then the temperature dependence of the order parameter is (*45*)

$$\frac{d(1 - S)}{dT} = \frac{3}{2}\frac{d}{dT}\langle\theta^2\rangle = \frac{3}{2T^*} \quad (11)$$

where, as described by Palmer and co-workers (*45*), T^* defines the characteristic temperature that represents the density of energy states thermally accessible to the bond vector and θ is the angle of deviation, not to be confused with θ from model-free results given above. If $T^*/T \leq 1$, then many additional conformational states are accessible to the N−H bond vector and the C_p of that conformational state resides in the classical limit. However, if $T^*/T \gg 1$, few additional states are thermally accessible and the conformation therefore has a low heat capacity.

RESULTS

Ligand Binding to RNase A. The synthesis of pTppAp was achieved with slight modifications of published procedures (*49*). Successful synthesis of pTppAp was confirmed by two-dimensional $^1H-^1H$ COSY and $^1H-^{31}P$ NMR COSY, which showed only the expected resonances, as well as negative mode electrospray mass spectrometry, which yielded an experimental mass, $M^{3-} = 269.4$ (theoretical 269.3) (see Supporting Information). The chemical structure of this molecule is depicted in Scheme 1.

Binding of pTppAp and 2′-CMP was quantitated using isothermal titration calorimetry under identical pH conditions (MES buffer, pH 6.4, 10 mM NaCl) as the subsequent NMR experiments. CMP binding was performed as a control and for comparison with thermodynamic values obtained for pTppAp. Shown in Figure 1 is the calorimetric titration of RNase A with pTppAp and 2′-CMP at 298 K. The calorimetric titration data were fit to eq 1 to yield thermodynamic values associated with ligand binding to RNase A. The product state analogue, 2′-CMP, binds to RNase A with a dissociation constant (K_d) of 3.6 ± 0.2 μM, a $\Delta H^\circ = -62.3 \pm 0.9$ kJ/mol, and a stoichiometry of 0.94 ± 0.01, which is in good agreement with literature values (*74*). The inhibitor, pTppAp, binds with higher affinity to RNase A than 2′-CMP at 298 K with thermodynamic constants, $K_d = 16.2 \pm 2.3$ nM, $\Delta H^\circ = -60.1 \pm 4.1$ kJ/mol, and a stoichiometry of 0.95 ± 0.05. Using eqs 3 and 4, the following values for ΔG° and $T\Delta S^\circ$ were calculated at 298 K for 2′-CMP and

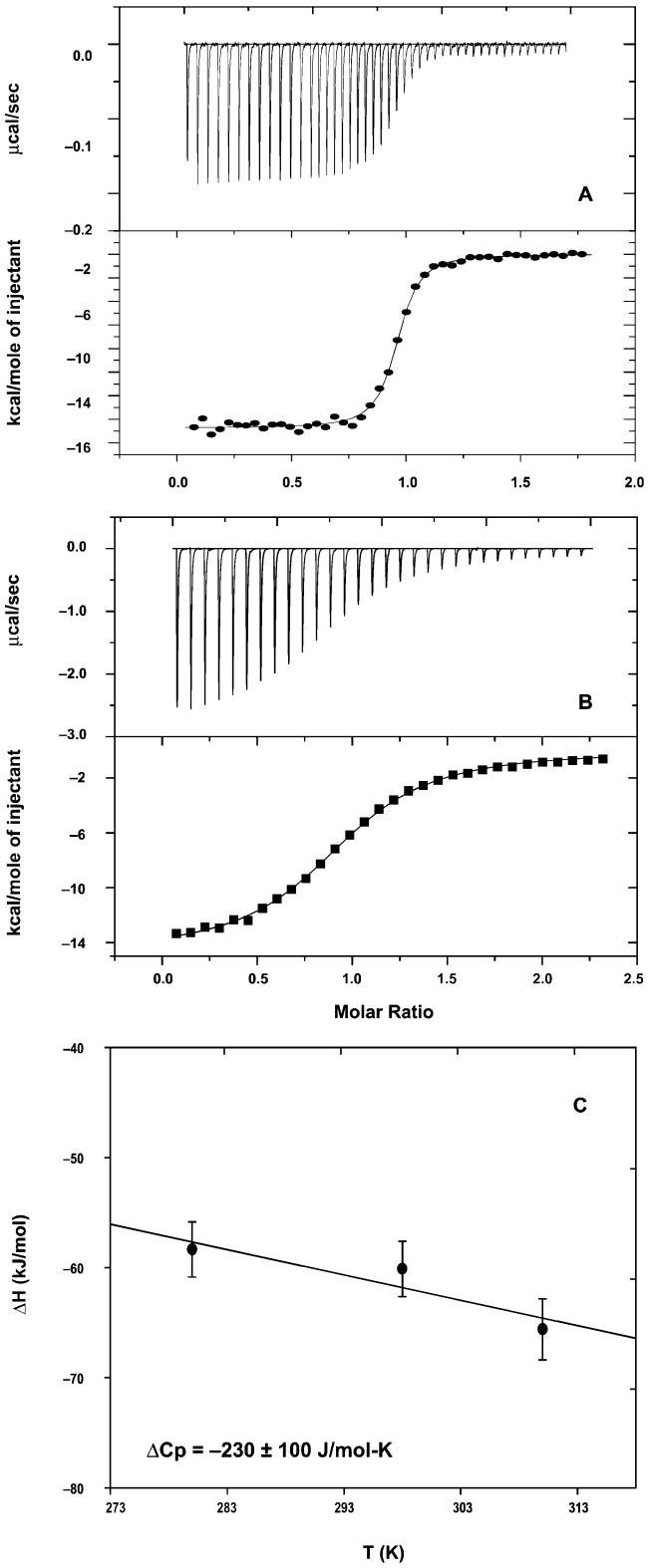

FIGURE 1: Ligand binding to RNase A. Titration calorimetry was used to monitor the binding of (A) pTppAp (ovals) and (B) 2′-CMP (squares) to RNase A. Binding studies were performed at 298 K in 20 mM MES buffer (pH 6.4). In A, [RNase A] = 2.8 μM, and in B, [RNase A] = 43.7 μM. The titration data were fitted to eq 1. (C) Heat capacity change from pTppAp binding to RNase A determined from separate experiments as described in Methods and Theory.

Table 1: Summary of Thermodynamic Values Determined for pTppAp Binding to RNase A[a]

temp (K)	K_d ($\times 10^{-9}$ M)[b]	ΔH (kJ/mol)[c]	ΔG (kJ/mol)[d]	$T\Delta S$ (kJ/mol)[e]
280	ND	-58.3 ± 2.5	ND	ND
288	7.9 ± 1.2	-59.5 ± 1.0	-44.7 ± 6.7	-14.8 ± 6.8
298	16.2 ± 2.3	-60.1 ± 4.1	-43.3 ± 6.1	-16.8 ± 7.3
311	33.4 ± 1.0	-66.0 ± 3.0	-44.4 ± 0.8	-21.6 ± 3.1

[a] All thermodynamic values are the average of multiple measurements, and reported uncertainties are the deviations of these multiple measurements from the average value. [b] Dissociation constants were determined from fits of calorimetric binding data. [c] Enthalpies were determined from separate experiments with excess RNase A as described in Methods and Theory. The enthalpy value at 288 K was determined from fits to titration data. [d] Binding energies were obtained from eq 3. [e] Entropies of binding were calculated using eq 4.

pTppAp, respectively: $\Delta G^\circ = -31.0 \pm 0.1$ and -43.3 ± 6.1 kJ/mol; $T\Delta S^\circ = -31.3 \pm 0.9$ and -16.8 ± 7.3 kJ/mol. For pTppAp, binding was measured as a function of temperature and the data are shown in Table 1 and Figure 1C. The heat capacity change (ΔC_p) for the interaction between pTppAp and RNase A was determined from the slope of the fitted line (Figure 1C) to be $\Delta C_p = -230 \pm 100$ J mol^{-1} K^{-1}. For comparison, ΔC_p for the pTppAp/RNase A interaction was estimated from burial of polar and nonpolar surface area upon ligand binding. Binding of pTppAp by RNase A buries 1639 Å^2 of surface area, which can be partitioned into 1010 and 629 Å^2 of nonpolar and polar groups, respectively. These values yield a theoretical ΔC_p of -1100 J mol^{-1} K^{-1} (*52*, *53*) for binding of pTppAp. For comparison, the experimental ΔC_p for 2′-CMP binding to RNase A is $\Delta C_p = -670$ (*75*) and -970 J mol^{-1} K^{-1} (*76*).

NMR Studies (Interaction between RNase A and pTppAp). After the characterization of the binding of pTppAp to RNase A, NMR experiments for apo and pTppAp-bound RNase A were initiated. Formation of the RNase A/pTppAp complex resulted in changes in chemical shifts for the backbone amide resonances for many amino acid residues. Addition of excess pTppAp (>1:1 pTppAp:RNase A) to RNase A resulted in no additional significant changes in amide peak positions. The results of this experiment are shown in Figure 2, in which the changes in ^{1}H and ^{15}N chemical shifts, upon interaction between RNase A and pTppAp, are mapped onto the RNase A structure.

NMR Studies (Backbone Dynamics). NMR spin-relaxation experiments were performed at 294, 301, and 311 K to characterize the temperature dependence of internal protein dynamics in RNase A in the apo and pTppAp form. To achieve this, measurements of R_1, R_2, NOE, and η_{xy} were performed at each temperature for RNase A and the RNase A/pTppAp complex (Supporting Information). For the apo enzyme, spin-relaxation data could be reliably quantitated for 102, 104, and 102 backbone amide positions of the 120 nonproline residues at 294, 301, and 311 K, respectively. For the pTppAp enzyme complex, the number of residues in which spin-relaxation data could be reliably quantitated was 93, 96, and 97 at the respective temperatures. The 10% trimmed average R_1, R_2, NOE, and η_{xy} values for apo RNase A and the RNase A/pTppAp complex at each temperature are given in Table 2. The nearly complete set of spin-relaxation rates at the three temperatures allowed model-free analysis to be performed at each. The resulting dynamics parameters for apo RNase A at 294, 301, and 311 K were $\tau_m = 8.20 \pm 0.02$, 6.61 ± 0.01, and 5.30 ± 0.01 ns, while at all temperatures $D_\parallel/D_\perp = 1.30$, $\theta = 86°$, and $\phi = 240$ (vide infra). Similar analysis of the RNase A/pTppAp complex gave values of $\tau_m = 9.02 \pm 0.02$, 6.80 ± 0.01, and 6.00 ± 0.01 ns at 294, 301, and 311 K, respectively, with $D_\parallel/D_\perp = 1.27$, $\theta = 78°$, and $\phi = 240$.

Table 2: Summary of NMR Spin-Relaxation Rates for RNase A in apo and pTppAp Forms

temp (K)	R_1 (s^{-1})	R_2 (s^{-1})	NOE	η_{xy} (s^{-1})
		apo RNase A		
294	1.44 ± 0.08	11.18 ± 1.74	0.780 ± 0.043	7.30 ± 0.62
301	1.66 ± 0.07	9.43 ± 1.77	0.777 ± 0.037	6.32 ± 0.53
311	1.89 ± 0.09	8.00 ± 1.98	0.770 ± 0.033	5.14 ± 0.44
		RNase A/pTppAp		
294	1.35 ± 0.07	13.26 ± 1.73	0.773 ± 0.045	8.29 ± 0.80
301	1.74 ± 0.08	10.10 ± 1.65	0.775 ± 0.041	6.71 ± 0.55
311	1.84 ± 0.09	9.06 ± 1.99	0.778 ± 0.043	5.35 ± 0.44

Apo RNase A. At 294 K, 88 residues were assigned to model 1, 13 to model 3, and one to model 4 as described by eq 8. At 301 K, 72 residues were fit to model 1, 30 to model 3, and two residues (Ser22 and Ser80) could not be fit with any model. At 310 K, 64 residues required model 1 and 38 residues were best fit by model 3. Over the full temperature range for RNase A, 72 residues are assigned to the same model. Generalized order parameters were determined for each of the resonances described above that could be reliably fit to models 1−5. Figure 3 depicts the S^2 values for each residue at 294, 301, and 311 K. The mean S^2 values for all quantifiable residues at 294, 301, and 311 K are 0.887 ± 0.015, 0.867 ± 0.011, and 0.851 ± 0.013, respectively. In Figure 4, the S^2 values for individual residues are color-coded onto the RNase A ribbon structure. Many residues were observed to be involved in a conformational exchange process, indicated by the necessary inclusion of a nonzero R_{ex} term in the model-free fitting. The number of residues for which $R_{ex} > 0$ increased from 13 to 30 to 38 as the temperature was increased from 294 to 301 to 311 K (Figure 3).

RNase A/pTppAp Complex. Upon formation of the RNase A/pTppAp complex, numerous amide resonances in RNase A experience changes in chemical shift that are localized at the enzyme active site (Figure 2). Several resonances disappear presumably due to exchange broadening. NOESY−HSQC experiments (*77*−*79*) were performed to reassign ambiguous resonances in the RNase A/pTppAp complex. After resonance assignment, identical NMR spin-relaxation experiments and model-free analysis were performed on the RNase A/pTppAp complex as for apo RNase A. For the pTppAp complex, 71 residues were assigned to model 1, 21 to model 3, and one to model 4, and one residue (Thr17) was not fit by any model at 294 K. At 301 K, 71 residues were fit to model 1, 25 to model 3, and one residue (Ser16) could not be fit with any model. At 311 K, 77 residues required model 1 and 20 residues were best fit by model 3. For the RNase A/pTppAp complex, 77 residues are assigned to the same model at all temperatures. Generalized order parameters were determined for each of the resonances described above that could be reliably fit to models 1−5. The average S^2 values at 294, 301, and 311 K for the

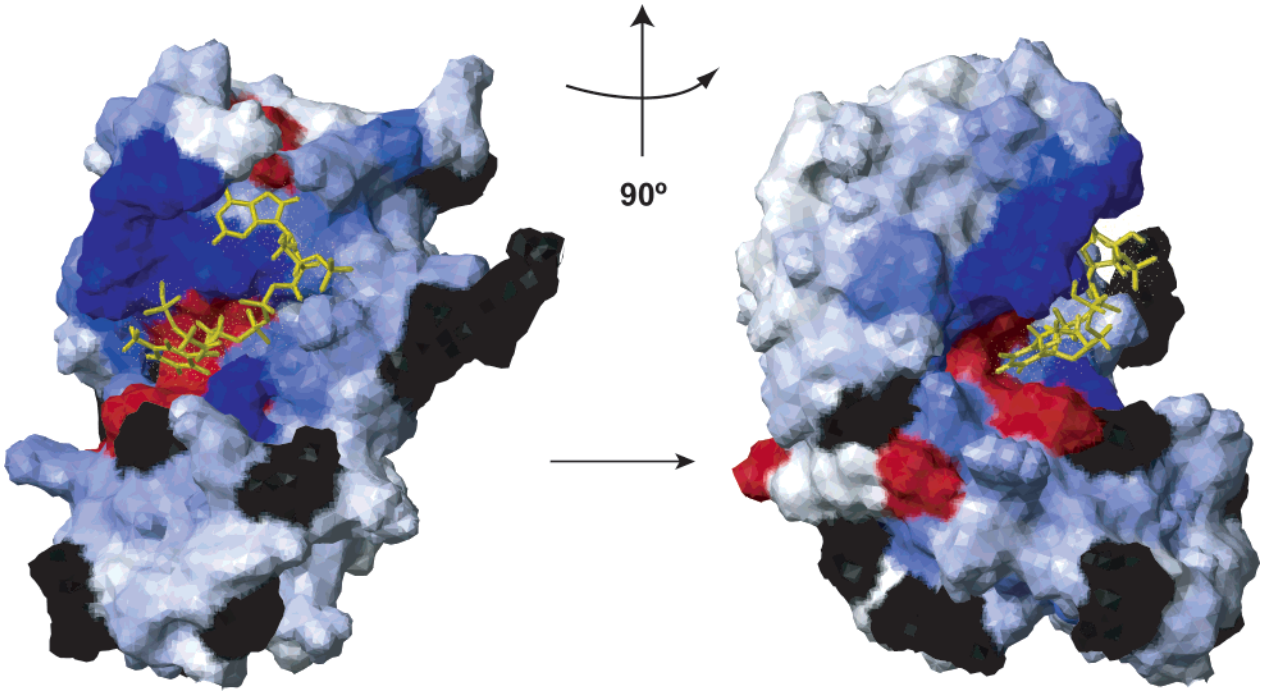

FIGURE 2: Spatial localization of altered $^{1}H-^{15}N$ chemical shifts in RNase A. The changes in chemical shift are mapped onto the van der Waals surface of RNase A. The surface is color-coded to reflect the magnitude, Δ, of chemical shift changes upon interaction with pTppAp. The value, $\Delta = \sqrt{(\Delta\delta_{NH}^2 + \Delta\delta_N^2/25)}/2$ reflects the average chemical shift change upon ligand binding in which $\Delta\delta_{NH}$ and $\Delta\delta_N$ are the chemical shift differences for the ^{1}H and ^{15}N atoms between the apo and the RNase A/pTppAp complex (*97*). Chemical shift values with $\Delta > 0.2$ are indicated in dark blue with linear interpolation from blue to white for $0.2 > \Delta > 0$. Resonances that disappear in the HSQC upon binding pTppAp are colored red and are presumed to be exchange broadened. Amino acids colored black are prolines or unassigned residues. The structure of the inhibitor, pTppAp, is shown in yellow and surrounded by dots representing its van der Waals surface. The placement of pTppAp at this location is based upon the crystal structure of a similar ligand (pdUppAp) bound to RNase A as described in the text. The two figures are related by a 90° rotation.

inhibited form of RNase A are 0.924 ± 0.016, 0.922 ± 0.018, and 0.901 ± 0.013, respectively. The values of S^2 for each amino acid residue in the inhibited RNase A/pTppAp complex at 294, 301, and 311 K are shown in Figure 3. In contrast to the results with apo RNase A, the number of residues for which a chemical exchange term was required for model-free fitting does not increase substantially with increasing temperature. These results are depicted in Figure 3. For comparison with apo RNase A, the order parameters for the pTppAp complex are color-coded onto the RNase A ribbon structure (Figure 4).

Temperature Dependence of S^2. The order parameters for residues in RNase A are dependent upon the experimental temperature. The value of S^2 decreases with increasing temperature for apo RNase A and for RNase A/pTppAp. Figure 5A shows the reduction in the average value of S^2 for all residues in RNase A as temperature increases. A similar plot is shown in Figure 5B in which only residues with the same motional model at all temperatures were included in the calculation of the mean S^2 value. The identical slopes of the lines in Figure 5 indicate that the overall temperature dependence of S^2 does not change significantly between apo and pTppAp forms of RNase A. However, on a residue-by-residue basis, this is not the case. Figure 6 shows the temperature dependence of the order parameter for residues in α-helix 1, loop 2, and β-sheet 5. A comparison of changes in order parameter with temperature for apo and pTppAp RNase A shows that differences exist on a per residue basis. The values of $d(1 - S)/dT$ for the residues shown in Figure 6 are for Gln11: $7.5 \pm 0.4 \times 10^{-4}$ K^{-1}, $2.9 \pm 2.6 \times 10^{-4}$ K^{-1}; for Lys41: $2.0 \pm 0.7 \times 10^{-3}$ K^{-1}, $1.6 \pm 0.2 \times 10^{-3}$ K^{-1}; and for Thr99: $0.2 \pm 0.1 \times 10^{-3}$ K^{-1}, $1.5 \pm 0.1 \times 10^{-3}$ K^{-1} for RNase A and RNase A/pTppAp, respectively. Equation 11 was used to calculate the characteristic temperature, T^*, for these residues. For the apo and inhibited forms of RNase A, these values are for Gln11: ~2000, 5000 K; for Lys41: ~750 and 940 K; and for Thr99: ~7500 and 1000 K, respectively. The variability of $d(1 - S)/dT$ grouped by 2° structure is shown as a box plot in Figure 7.

DISCUSSION

The use of substrate mimics or enzyme inhibitors is often used to study enzymatic reaction mechanisms. This approach has not widely been exploited to address the role of protein dynamics in enzyme function. As an initial step in this area, we have compared and characterized the temperature dependence of the dynamics in RNase A in the ground and pTppAp-bound states. The construction of pyrophosphate-based ligands such as pTppAp was originally suggested by the observation, from kinetic inhibition studies, that 5′-ADP (ppA) bound to RNase A 70-fold tighter than 5′-AMP (pA) (*80*). Chemical elaboration of the core ppA molecule yielded several nanomolar affinity dinucleotide inhibitors containing the pyrophosphate linkage. Subsequently, a high-resolution crystal structure of one of these inhibitors, pdUppA-3′-p, bound to RNase A was solved (*56*). Several features of this complex are worth noting. The 5′-β-phosphate occupies the P1 (cleavage) site, and the adenine ring (normally in the anti configuration in the RNase A/substrate complex) is rotated

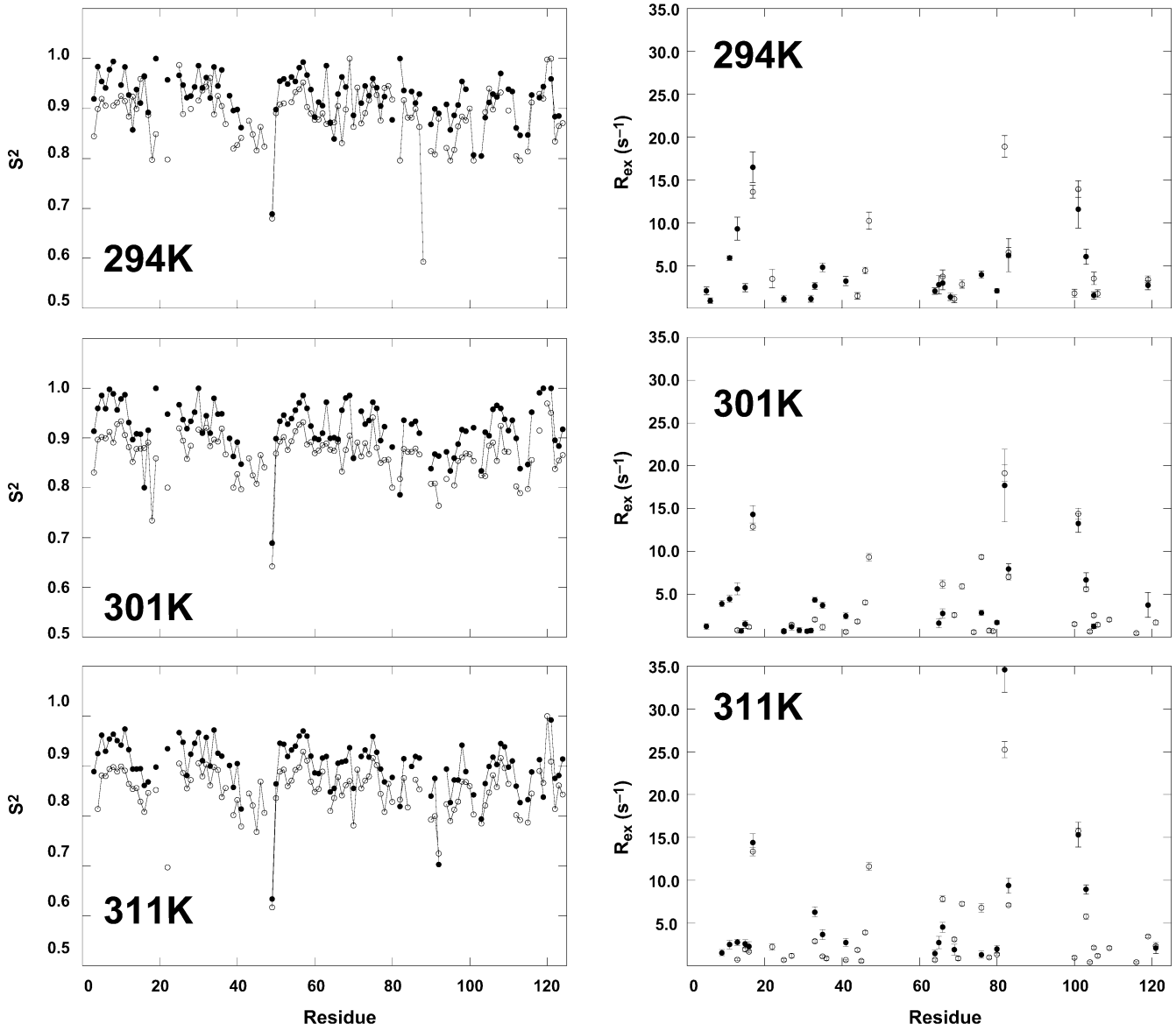

FIGURE 3: Temperature dependence of dynamical parameters for RNase A. The results of model-free analysis for apo RNase A (open circles) and the inhibited RNase A/pTppAp complex (filled circles) are depicted. On the left, order parameters, S^2, are shown as a function of the amino acid primary sequence and experimental temperature. On the right, amino acid residues that exhibit chemical exchange (R_{ex}) are shown. Breaks in the lines indicate residues in which quantitation of dynamical parameters was not possible. Error bars have been removed to aid in visualization of the data trends. Uncertainties in S^2 values for the data shown above, in all cases, is ~1−2%.

nearly 180° into the syn conformation. Despite these differences in bound ligand conformation, nearly all observed enzyme−substrate interactions exist in the pyrophosphate complexes. In specific, the exocyclic amino group of the adenine ring is in a similar position as it is in the normal substrate and makes hydrogen bonds with Asn71, Asn67, and Gln69 at the B2 subsite. The β-phosphate makes similar contacts (Gln11, His12, Lys41, His119, and Phe120) as those formed by the α-phosphate at the P1 site with the normal, monophosphate nucleotide ligands. In addition, the location of the β-phosphate is very similar to that occupied by the oxyvanadate anion in the RNase A/uridyl vanadate complex. The uracil base forms identical hydrogen bonds as uridyl vanadate with Thr45 at the B1 subsite, and the terminal 5′-phosphate interacts weakly with Lys66. Thus, the majority of the canonical ligand/enzyme interactions is realized in the structurally characterized dinucleotide pyrophosphate complex. While no structure of the RNase A/pTppAp complex has been reported, we anticipate, given the similarities in structure and affinity for RNase A, that pTppAp and pdUppA-3′-p occupy the active site in a comparable fashion. Furthermore, addition of pTppAp to ^{15}N-labeled RNase A results in changes in the chemical shifts for a significant number of residues suggesting their interaction with the inhibitor. The largest changes occur in the active site region and localizes to β-sheets 1, 4, 5, 6, and loop 4, which includes the B2 and P0 subsites (Figure 2 and Scheme 1). Resonances for residues 43−48 located in β-sheet 1 are absent in spectra of the RNase A/pTppAp complex, a fact that may be attributable to exchange broadening. The latter set of residues also shows large pH-dependent chemical shift changes in apo RNase A (*15*). As a whole, the pattern of chemical shift changes is consistent with pTppAp binding at the RNase A active site (Figure 2). In addition, pTppAp is an inhibitor against the RNase A-catalyzed cleavage of cytidylyl(3′,5′)-guanosine (*49*). On the basis of these observations, we have modeled the thymidine moiety of pTppAp into the RNase A active site using the structure of pdUppA-3′-p bound to

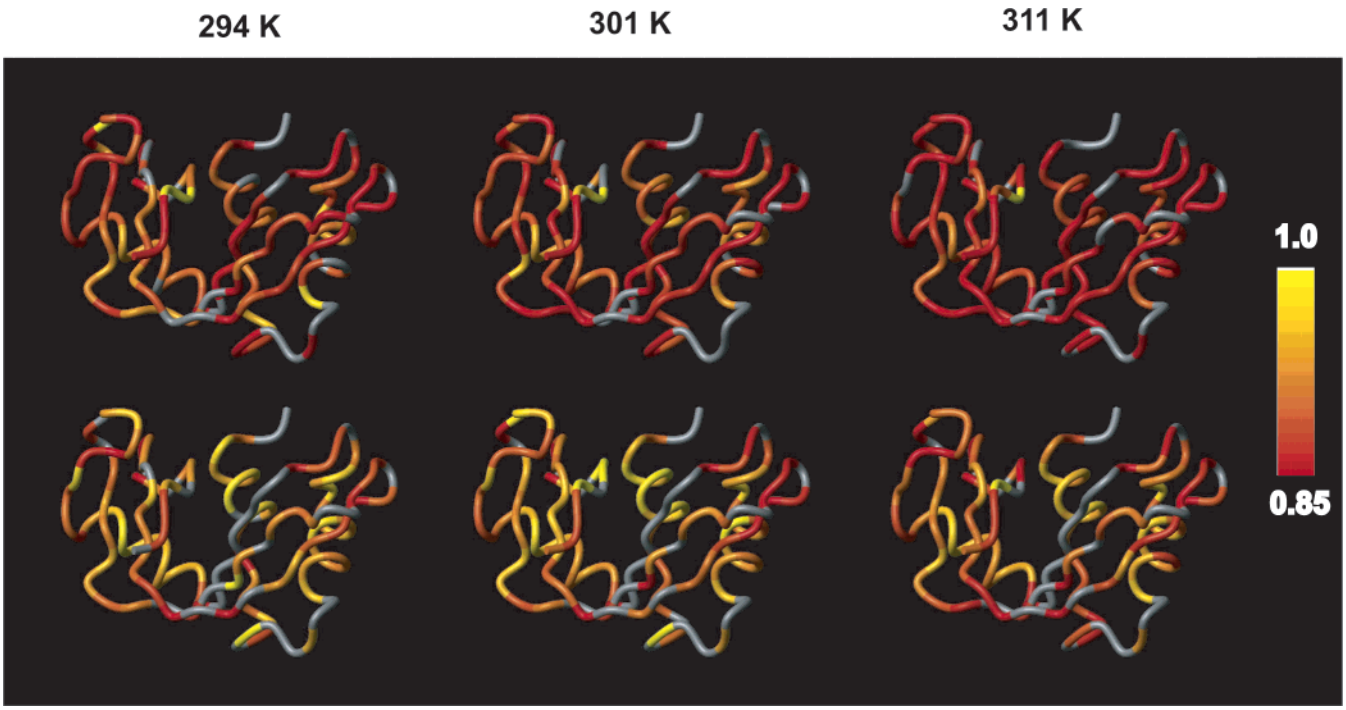

FIGURE 4: Temperature dependence of dynamical parameters for RNase A. Values of S^2 are colored onto ribbon representation of the RNase A structure. S^2 results for apo RNase A are shown in the top panel, while the bottom panel pertains to the RNase A/pTppAp complex. The color scheme for the order parameters is shown by the bar at the right of the figure and is represented by red for $S^2 < 0.85$ and linearly interpolated to yellow at $S^2 = 1.0$. Gray represents proline residues and residues in which low signal-to-noise or overlap prevented reliable quantitation of S^2.

RNase A as a scaffold (Figure 2). The pyrophosphate ligands are not strict mimics of the transition state; yet, they do interact with RNase A with 10^4-fold and 50-fold greater affinity than the corresponding dinucleotide substrate (*46*) and transition state analogue uridine 2′,3′-cyclic vanadate (*81*, *82*) and thus combine with the enzyme to form a higher energy enzyme complex. RNase A and pTppAp interact with nanomolar affinity over the temperature range studied. Furthermore, calorimetric measurement of these dissociation constants agrees with values determined from kinetic inhibition studies (*49*). Tight binding is also supported by NMR results in which no significant changes in amide chemical shifts are observed above a 1:1 stoichiometric mixture of pTppAp and RNase A. The main determinant of the increased binding affinity of pTppAp appears to be entropic in origin $\Delta(T\Delta S) = [(T\Delta S_{pTppAp}) - (T\Delta S_{CMP})] = 14.5 \pm 7.4$ kJ/mol.

Temperature Dependence of Motional Parameters. The internal amide backbone dynamics were determined at three temperatures for apo RNase A and RNase A/pTppAp. Typically, protein dynamics derived from model-free analysis are discussed in terms of two time scales: (i) the μs−ms time scale, which is characterized by the exchange broadening parameter, R_{ex}, and (ii) motional amplitude of the amide N−H bond vector on the ps−ns time scale described by the generalized order parameter, S^2.

Conformational Exchange (μs−ms Motion). Chemical exchange broadening of resonances occurs throughout the apo RNase A structure, consistent with previously reported relaxation-compensated CPMG measurements (*15*), which indicated the occurrence of a global concerted motional process with a rate constant of ca. 1600 s^{-1}. In the present work, some amino acid residues such as Gln101 have similar temperature dependencies of R_{ex} in both enzyme forms. Glutamine 101 exhibits an increase in R_{ex} as the sample temperature increases, whereas other residues such as Thr17 display a decrease in R_{ex} with increasing temperature. Overall, the temperature dependence of R_{ex} for residues in RNase A does not differ significantly between the apo and the pTppAp forms, suggesting that inhibitor binding does not substantially affect backbone mobility on the μs−ms time scale. Notable exceptions are residues Gln11 and Met13. In the apo enzyme, Gln11 requires no R_{ex} term for successful model-free fitting at any of the temperatures. Yet, in the pTppAp/enzyme complex, Gln11 experiences a conformational exchange process at all three temperatures in which the value of R_{ex} decreases as the temperature is increased. Likewise, methionine 13 (apo RNase A) exhibits no chemical exchange behavior at 294 K and requires a small (<1 s^{-1}) R_{ex} term at 301 and 311 K. In contrast, when pTppAp is bound, Met13 has R_{ex} values of 9.3 ± 1.3, 5.6 ± 0.7, and 2.5 ± 0.4 s^{-1} at 294, 301, and 311 K, respectively. Glutamine 11 and Met13 are both located at the enzyme active site; therefore, their dynamics are likely responding to the effects of ligand binding. In a straightforward scenario, an increase in R_{ex} with temperature suggests a transition from the slow exchange regime to that of intermediate exchange, while a decrease in R_{ex} with increasing temperature implies a shift to the fast exchange time scale (*83*). However, interpretation of chemical exchange is often complicated because the populations, chemical shift differences, and kinetics, which contribute to the R_{ex}, are usually not known (*84*). A more detailed description of these effects will require additional experiments (*85*), which are in progress. Overall, these studies imply that the binding of pTppAp does not significantly alter the μs−ms dynamic processes in RNase A. This effect has been noted in other enzyme systems, such as for the enzyme triosephosphate isomerase in which ligand bound

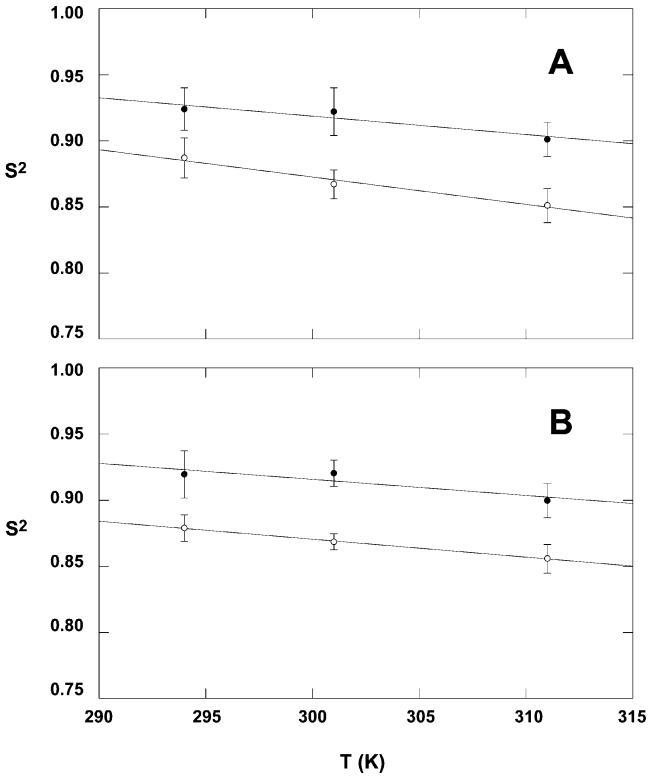

FIGURE 5: Temperature dependence of the average S^2 for RNase A. The overall average value of S^2 for RNase A is shown as a function of temperature for apo RNase A (open circles) and RNase A/pTppAp (filled circles). In A, S^2 was calculated by averaging all of the S^2 values from the model-free results. In B, the average S^2 value was determined only for residues that exhibit the same motional model over the entire temperature range. The slope of the lines for all four data sets is within experimental error.

to the active site did not affect the kinetics of the active site loop motion (*36*).

Comparison of S^2 for Apo and Liganded RNase A (ps−ns Motion). In contrast to the minor changes in conformational exchange processes caused by pTppAp binding, significant differences in motional dynamics on the ps−ns time scale are observed between the apo RNase A and the RNase A/pTppAp enzyme forms. The order parameters, for residues in the pTppAp complex, are clearly elevated relative to uninhibited ribonuclease A, indicating a rigidification of the protein backbone upon ligand binding. The increase in S^2 values due to the presence of ligand is observed for all of the highly conserved, catalytically important residues in RNase A including K7, Q11, H12, K41, K66, N71, D83, E111, H119, and D121. Of these, the observation of motional restriction of K41 in the presence of ligand concurs with previous neutron diffraction studies (*86*). However, decreased mobility is not localized solely to the residues at the enzyme active site and as depicted in Figures 3 and 4 occur throughout the protein structure. The difference in the overall average S^2 values between the apo and the inhibited RNase A ($S^2_{apo} - S^2_{pTppAp}$) at 294, 301, and 311 K is −0.037, −0.055, and −0.050, respectively. These differences in S^2 values, between the two enzyme forms, implies an average decrease in N−H bond vector mobility of ∼3−4° upon pTppAp binding, assuming a restricted diffusion in a cone motional model (*65*, *87*). The freezing of motion upon ligand binding has been documented previously. Fushman et al. showed that the backbone mobility in certain regions of ribonuclease T1 decreases upon binding of GMP (*20*). For the enzyme oxalocrotonate tautomerase both an increase and a decrease in S^2 values was observed upon inhibitor binding (*88*). In that work, the authors suggested that residues with increased mobility as a consequence of inhibitor binding reduced the total entropic penalty for the ordering of other residues. In contrast, observations on RNase A indicate that the decrease in mobility caused by pTppAp binding occurs throughout the enzyme.

Temperature Dependence of S^2. Considering only the average S^2 for RNase A and RNase A/pTppAp reveals that ligand binding has no apparent effect on the temperature dependence of these values, i.e., the lines in Figure 5 are parallel. S^2 and configurational entropy are related; therefore, the identical temperature dependence of S^2 (and entropy) for the two enzyme forms indicates no contribution to changes in heat capacity originates from the backbone dynamics. However, as shown in Figure 6, changes in the temperature dependence of the order parameter do exist at the level of individual amino acid residues. These differences are such that there is an overall cancellation of positive and negative contributions to the total heat capacity change, resulting in no net contribution to ΔC_p. This implies that there is a complex redistribution of the backbone energetics upon pTppAp binding and an alteration of the protein energy landscape. However, these NMR studies suggest that changes in backbone dynamics contribute little to the overall ΔC_p for RNase A/pTppAp interaction and the net heat capacity change for binding pTppAp (−230 J/mol K) must arise from other sources (*89*). As mentioned above, examination of the temperature dependence of S^2 for individual residues reveals site specific differences between free and pTppAp-bound RNase A. A weaker dependence of S^2 on temperature implies a reduction in the thermally accessible states available to a particular residue (i.e., the residue has a larger characteristic temperature, T^*, or similarly a reduced local heat capacity) (*45*). For example, the S^2 values for Gln11 (in α-helix1) have a weaker temperature dependence in the pTppAp complex than in the free enzyme. When bound to ligand, Gln11 has access to fewer conformational states than in apo RNase A; the opposite is true for Thr99. For many residues, there is no substantial change in $d(1 - S)/dT$. The observed decrease in the slope of $(1 - S)$ with temperature for certain residues in RNase A/pTppAp relative to apo RNase A implies a flattening of the bottom of the potential energy well for these residues. Thus, the temperature dependence of S^2 provides constraints to the potential energy function describing the motional process (*38*, *39*, *45*).

Interestingly, grouping of $d(1 - S)/dT$ values by secondary structure element shows a marked reduction in the variation of these values for RNase A/pTppAp relative to apo RNase A. This is depicted in Figure 7 in box plot form (*90*). The box plot allows simultaneous visualization of the median value of a set of measurements, their variability, as well as asymmetry in the data and data outliers. Figure 7 highlights two main differences in the response of $(1 - S)$ to temperature. First, there is a decrease in the median $d(1 - S)/dT$ values for several regions of 2° structure in the inhibited complex. Second, the spread in $d(1 - S)/dT$ values is significantly reduced for RNase A/pTppAp relative to apo RNase A, indicating a reduced dynamic for the RNase A/pTppAp complex and a redistribution of the backbone

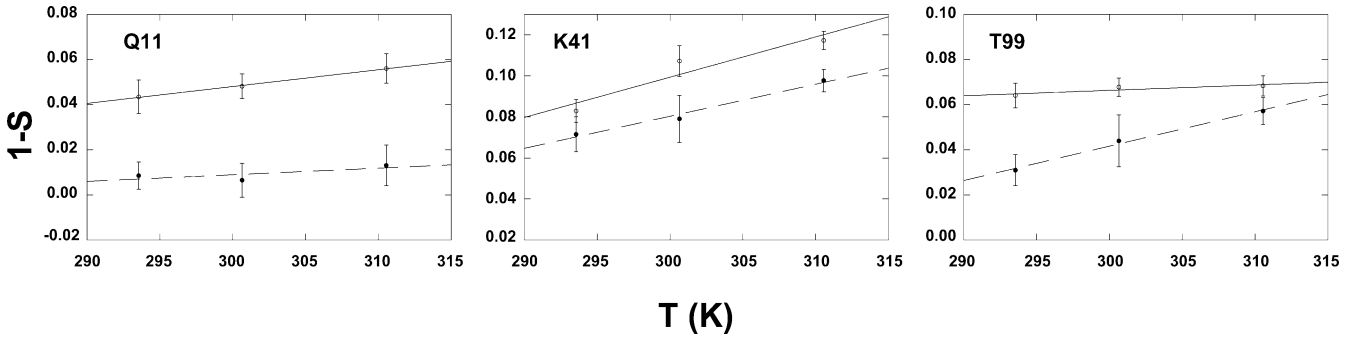

FIGURE 6: Temperature dependence of the order parameters for RNase A. The values of 1-S for glutamine 11, lysine 41, and threonine 99 are shown as a function of temperature for apo RNase A (open circles/solid lines) and RNase A/pTppAp (filled circles/dashed lines). These residues represent three different elements of 2° structure: α-helix 1 (Gln11), loop 2 (Lys41), and *β*-sheet 5 (Thr99). The slopes of the fitted lines are Gln11: $7.5 \pm 0.4 \times 10^{-4}$ K^{-1}, $2.9 \pm 2.6 \times 10^{-4}$ K^{-1}; Lys41: $2.0 \pm 0.7 \times 10^{-3}$ K^{-1}, $1.6 \pm 0.2 \times 10^{-3}$ K^{-1}; and Thr99: $0.2 \pm 0.1 \times 10^{-3}$ K^{-1}, $1.5 \pm 0.1 \times 10^{-3}$ K^{-1} for apo and RNase A/pTppAp, respectively.

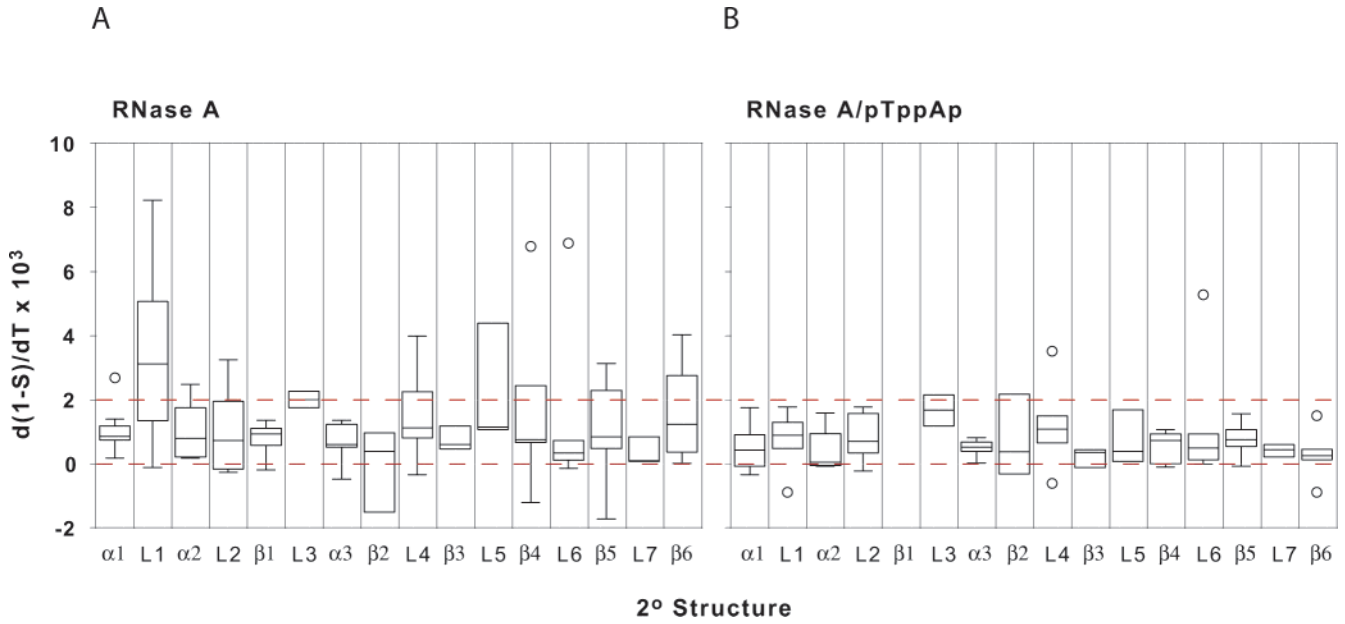

FIGURE 7: Distribution of d(1 − *S*)/d*T* for RNase A 2° structure. The variation in d(1 − *S*)/d*T* within each secondary structure element in RNase A is depicted in the box plots for (A) apo RNase A and (B) RNase A/pTppAp. Elements of 2° structure are arranged in order of occurrence in the RNase A primary structure. The bar inside the box indicates the median value of d(1 − *S*)/d*T*, while the ends of the box mark boundaries with the upper and lower quartile of the data, and the bars extending from the box indicate the minimum and maximum data values. The circles represent outliers in the data set, specified as points whose value is either greater than upper quartile + 1.5 × IQD or less than lower quartile − 1.5 × IQD, in which IQD (interquartile distance) is defined as the upper quartile − lower quartile. The ratio of the number of residues from each 2° structure element used in the box plot relative to the total number of nonproline residues in that segment of 2° structure for apo RNase A (RNase A/pTppAp) is α-1, 9(9)/9; loop-1, 8(6)/12; α-2, 7(8)/8; loop-2, 8(8)/9; *β*-1, 5(0)/5; loop-3, 2(2)/3; α-3, 9(9)/9; *β*-2, 4(4)/4; loop-4, 8(7)/8; *β*-3, 3(3)/3; loop-5, 4(4)/4; *β*-4, 7(5)/8; loop-6, 7(7)/9; *β*-5, 13(13)/15; loop-7, 3(3)/3; *β*-6, 7(6)/7. The d(1 − *S*)/d*T* values presented in this plot represent all residues in which S^2 could be quantitated over the full temperature range. The dashed red lines are drawn to aid in comparison of plots A and B only.

energetics. This is especially apparent for loops 1 and 5, *β*-sheets 4−6, and to a lesser extent α-helix 3. When bound to ligand, the dynamics of these regions of the enzyme possess a more uniform response to temperature than in the absence of ligand. This implies that the energy landscape for individual regions in RNase A/pTppAp is very different from that of apo RNase A and suggests that optimization of binding interactions may be achieved by altering the protein dynamics in specific protein regions, through mutagenesis for instance.

NMR and Entropy. The total entropy change (Δ*S*°) for the interaction between protein and ligand can be measured by titration calorimetry and partitioned as

$$\Delta S^\circ = \Delta S_{conf} + \Delta S_{hyd} + \Delta S_{RT} \qquad (12)$$

in which ΔS_{hyd} is the entropy change due to changes in hydration of protein and ligand, ΔS_{RT} is the change in translational/rotational entropy, both ΔS_{hyd} and ΔS_{RT} can be estimated, and ΔS_{conf} is the change in configurational entropy of the protein and ligand and is trivially determined once ΔS°, ΔS_{hyd}, and ΔS_{RT} are known. Alternatively, ΔS_{conf} for the protein can be obtained from NMR measurements (*38*, *39*, *42*) and subsequently compared to the calculated value. The change in rotational/translational entropy (ΔS_{RT}) for protein/ligand interactions has been estimated to be −210 J/mol K (*89*). To estimate ΔS_{hyd}, we use the data of Dubins et al. (*91*) who used volumetric studies to determine the release of 210 ± 40 water molecules upon RNase A/ligand binding. Using this value and small molecule thermodynamic transfer data (*92*, *93*), Dubins et al. calculate $\Delta S_{hyd} = 1130$

± 580 J/mol K. The ligand 2′-CMP was used in that study, not pTppAp, but given the more positive value of $\Delta S°$ for binding of pTppAp, this value is likely a lower limit estimate of ΔS_{hyd} for the RNase A/pTppAp interaction. Subtracting these values from the calorimetrically determined value for pTppAp ($\Delta S° = -56$ J/mol K) gives a value for $\Delta S^{est}_{conf} = -980$ J/mol K. This estimated value for the change in configurational entropy can be compared with the value determined by NMR spectroscopic measurements (*40*). Assuming the overall change in order parameters between the RNase A and the RNase A/pTppAp complex represents the average change per residue, then the room temperature change in configurational entropy determined from eq 9 is approximately −3.5 J/mol K residue. Summing this value over the number of residues (124 amino acids) in RNase A provides an NMR-derived entropy change associated with RNase A binding to pTppAp $\Delta S^{NMR}_{conf} = -430$ J/mol K, which represents ca. 44% of the value for ΔS^{est}_{conf} determined above. The NMR measurements in this study provide insight into the configurational entropy of the backbone only and do not account for contributions from amino acid side chains or the ligand. On the basis of these NMR results, the contribution from the side chains would therefore represent ∼56% of the total configurational entropy lost upon pTppAp binding, neglecting any contributions from the ligand. Theoretical considerations of protein folding indicate that the contribution to configurational entropy provided by the side chains is ∼55−60% (*94*, *95*); therefore, a 44% contribution from the backbone appears to be a reasonable estimate. The validity of solution NMR-determined thermodynamic quantities has been supported from an experimental and theoretical basis (*37*−*42*, *96*). The derivation of expressions for configurational entropy from NMR-derived order parameters assumes that individual bond vector motion is independent. In cases in which correlated motion exists, the determined entropy values are an overestimate of the true value. However, as Brüschweiler has recently shown, for ubiquitin, correlated motion surprisingly does not lead to a severe overestimation of entropy values (*96*). An additional concern with RNase A arises if ΔS_{hyd} is underestimated, a real possibility since pTppAp buries more nonpolar surface in its interaction with RNase A than 2′-CMP. The potential inequivalence of ΔS_{hyd} for 2′-CMP and pTppAp would result in an overestimation of the backbone contribution to ΔS_{conf}. On this basis, the estimated value of −430 J/mol K of configurational entropy, attributed here to the backbone of RNase A upon binding pTppAp, likely represents an upper limit.

CONCLUSIONS

Comparison of the temperature dependence of S^2 for RNase A in two enzyme forms demonstrates an overall rigidification of the protein backbone upon ligand binding. The change in backbone configurational entropy determined by NMR is in reasonable agreement with calorimetric values and with theoretical estimates for binding of pTppAp. The temperature dependence of the backbone dynamics for both enzyme forms indicates that while the backbone contributes little to the total overall heat capacity change for pTppAp binding, different regions of the enzyme respond differently to the presence of ligand. This redistribution of backbone energetics is complex; however, it generally appears that the spread in the temperature dependence of S^2 decreases and becomes more uniform in the presence of ligand.

ACKNOWLEDGMENT

We thank Professor Andrew Hamilton (Yale) for the use of the titration calorimeter, Professors Ann Valentine, Enrique De La Cruz, and Kurt Zilm for helpful suggestions, and Dr. James G. Kempf for critical reading of this manuscript. We thank Yale University for the purchase of the Varian 600 MHz NMR instrument used in these studies.

SUPPORTING INFORMATION AVAILABLE

Tabulated relaxation rates for apo and pTppAp RNase A at 294, 301, and 311 K, two-dimensional $^1H-^{31}P$ correlation spectrum of pTppAp, mass spectrum of pure pTppAp, and ^1H NMR spectrum used to measure pTppAp concentration. This material is available free of charge via the Internet at http://pubs.acs.org.

REFERENCES

1. delCardayre, S. B., and Raines, R. T. (1994) *Biochemistry 33*, 6031−6037.
2. Riordan, J. F. (1997) in *Ribonucleases: Structures and Functions* (D'Alessio, G., and Riordan, J. F., Eds.) pp 445−489, Academic Press, New York.
3. D'Alessio, G., Di Donato, A., Mazzarella, L., and Piccoli, R. (1997) in *Ribonucleases: Structures and Functions* (D'Alessio, G., and Riordan, J. F., Eds.) pp 383−423, Academic Press, New York.
4. Youle, R. J., and D'Alessio, G. (1997) in *Ribonucleases: Structures and Functions* (D'Alessio, G., and Riordan, J. F., Eds.) pp 491−514, Academic Press, New York.
5. Anfinsen, C. B. (1973) *Science 181*, 223−230.
6. Moore, S., and Stein, W. H. (1973) *Science 180*, 458−464.
7. Merrifield, B. (1986) *Science 232*, 341−347.
8. Kartha, G., Bello, J., and Harker, D. (1967) *Nature 213*, 862−865.
9. Rasmussen, B. F., Stock, A. M., Ringe, D., and Petsko, G. A. (1992) *Nature 357*, 423−424.
10. Raines, R. T. (1998) *Chem. Rev. 98*, 1045−1066.
11. Thompson, J. E., Kutateladze, M. C., Venegas, F. D., Messmore, J. M., and Raines, R. T. (1995) *Bioorg. Chem. 23*, 471−481.
12. Erman, J. E., and Hammes, G. G. (1966) *J. Am. Chem. Soc. 88*, 5607−5614.
13. Cathou, R. E., and Hammes, G. G. (1965) *J. Am. Chem. Soc. 86*, 3240−3245.
14. Hammes, G. G. (2002) *Biochemistry 41*, 8221−8228.
15. Cole, R., and Loria, J. P. (2002) *Biochemistry 41*, 6072−6081.
16. Pauling, L. (1948) *Nature 161*, 707−709.
17. Bruice, T. C., and Benkovic, S. J. (2000) *Biochemistry 39*, 6267−6274.
18. Young, L., and Post, C. B. (1996) *Biochemistry 35*, 15129−15133.
19. Cameron, C. E., and Benkovic, S. J. (1997) *Biochemistry 36*, 15792−15800.
20. Fushman, D., Weisemann, R., Thüring, H., and Rüterjans, H. (1994) *J. Biomol. NMR 4*, 61−78.
21. Mandel, A. M., Akke, M., and Palmer, A. G. (1995) *J. Mol. Biol. 246*, 144−163.
22. Shapiro, Y. E., Sinev, M. A., Sineva, E. V., Tugarinov, V., and Meirovitch, E. (2000) *Biochemistry 39*, 6634−6644.
23. Wang, L., Pang, Y., Holder, T., Brender, J. R., Kurochkin, A. V., and Zuiderweg, E. R. (2001) *Proc. Natl. Acad. Sci. U.S.A. 98*, 7684−7689.
24. Deng, H., Zhadin, N., and Callender, R. (2001) *Biochemistry 40*, 3767−3773.
25. Rader, S. D., and Agard, D. A. (1997) *Protein Sci. 6*, 1375−1386.
26. Tilton, R. F., Dewan, J. C., and Petsko, G. A. (1992) *Biochemistry 31*, 2469−2481.
27. Kohen, A., and Klinman, J. P. (2000) *J. Am. Chem. Soc. 122*, 10738−10739.

28. Antoniou, D., and Schwartz, S. D. (2001) *J. Phys. Chem. B. 105*, 5553−5558.
29. Radkiewicz, J. L., and Brooks, C. L. I. (2000) *J. Am. Chem. Soc. 122*, 225−231.
30. Villa, J., and Warshel, A. (2001) *J. Phys. Chem. B 105*, 7887−7907.
31. Ota, N., and Agard, D. A. (2001) *Protein Sci. 10*, 1403−1414.
32. Broos, J., Visser, A. J. W. G., Engbersen, J. F. J., Verboom, W., van Hoek, A., and Reinhoudt, D. N. (1995) *J. Am. Chem. Soc. 117*, 12657−12663.
33. Akerud, T., Thulin, E., Van Etten, R. L., and Akke, M. (2002) *J. Mol. Biol. 322*, 137−152.
34. Eisenmesser, E. Z., Bosco, D. A., Akke, M., and Kern, D. (2002) *Science 295*, 1520−1523.
35. Rozovsky, S., Jogl, G., Tong, L., and McDermott, A. E. (2001) *J. Mol. Biol. 310*, 271−280.
36. Williams, J. C., and McDermott, A. E. (1995) *Biochemistry 34*, 8309−8319.
37. Akke, M., Brüschweiler, R., and Palmer, A. G. (1993) *J. Am. Chem. Soc. 115*, 9832−9833.
38. Li, Z., Raychaudhuri, S., and Wand, A. J. (1996) *Protein Sci. 5*, 2647−2650.
39. Yang, D., and Kay, L. E. (1996) *J. Mol. Biol. 263*, 369−382.
40. Bracken, C., Carr, P. A., Cavanagh, J., and Palmer, A. G. (1999) *J. Mol. Biol. 285*, 2133−2146.
41. Seewald, M. J., Pichumani, K., Stowell, C., Tibbals, B. V., Regan, L., and Stone, M. J. (2000) *Protein Sci. 9*, 1177−1193.
42. Yang, D., Mok, Y. K., Forman-Kay, J. D., Farrow, N. A., and Kay, L. E. (1997) *J. Mol. Biol. 272*, 790−804.
43. Lee, A. L., and Wand, A. J. (2001) *Nature 411*, 501−504.
44. Lee, A. L., Sharp, K. A., Kranz, J. K., Song, X.-J., and Wand, A. J. (2002) *Biochemistry 41*, 13814−13825.
45. Mandel, A. M., Akke, M., and Palmer, A. G. (1996) *Biochemistry 35*, 16009−16023.
46. delCardayre, S. B., Ribo, M., Yokel, E. M., Quirk, D. J., Rutter, W. J., and Raines, R. T. (1995) *Protein Eng. 8*, 261−273.
47. Anderson, D. G., Hammes, G. G., and Walz, F. G., Jr. (1968) *Biochemistry 7*, 1637−1645.
48. Moffat, J. G., and Khorana, H. G. (1961) *J. Am. Chem. Soc. 83*, 663−675.
49. Russo, N., and Shapiro, R. (1999) *J. Biol. Chem. 274*, 14902−14908.
50. Son, T. D., and Chachaty, C. (1977) *Biochim. Biophys. Acta 500*, 405−418.
51. Jelesarov, I., and Bosshard, H. R. (1999) *J. Mol. Recognit. 12*, 3−18.
52. Spolar, R. S., Livingstone, J. R., and Record, M. T., Jr. (1992) *Biochemistry 31*, 3947−3955.
53. Murphy, K. P., and Freire, E. (1992) *Adv. Protein Chem. 43*, 313−361.
54. Hubbard, S. J., and Thornton, J. M. (1993) Department of Biochemistry and Molecular Biology, University College, London.
55. Wlodawer, A., Svensson, L. A., Sjolin, L., and Gilliland, G. L. (1988) *Biochemistry 27*, 2705−2717.
56. Leonidas, D. D., Shapiro, R., Irons, L. I., Russo, N., and Acharya, K. R. (1999) *Biochemistry 38*, 10287−10297.
57. Kordel, J., Skelton, N. J., Akke, M., Plamer, A. G., and Chazin, W. J. (1992) *Biochemistry 31*, 4856−4866.
58. Skelton, N. J., Palmer, A. G., Akke, M., Kördel, J., Rance, M., and Chazin, W. J. (1993) *J. Magn. Reson., Ser. B 102*, 253−264.
59. Kay, L. E., Keifer, P., and Saarinen, T. (1992) *J. Am. Chem. Soc. 114*, 10663−10665.
60. Kempf, J. G., and Loria, J. P. (2003) in *Protein NMR Techniques* (Downing, A. K., Ed.) Humana Press, Totowa, NJ (in press).
61. Kroenke, C. D., Loria, J. P., Lee, L. K., Rance, M., and Palmer, A. G. (1998) *J. Am. Chem. Soc. 120*, 7905−7915.
62. Tjandra, N., Szabo, A., and Bax, A. (1996) *J. Am. Chem. Soc. 118*, 6986−6991.
63. Delaglio, F., Grzesiak, S., Vuister, G., Zhu, G., Pfeifer, J., and Bax, A. (1995) *J. Biomol. NMR 6*, 277−293.
64. Goddard, T., and Kneller, D. G. *SPARKY 3*, University of California, San Francisco.
65. Lipari, G., and Szabo, A. (1982) *J. Am. Chem. Soc. 104*, 4546−4559.
66. Lipari, G., and Szabo, A. (1982) *J. Am. Chem. Soc. 104*, 4559−4570.
67. Cole, R., and Loria, J. P. (2003) *J. Biomol. NMR* (in press).
68. Palmer, A. G., Rance, M., and Wright, P. E. (1991) *J. Am. Chem. Soc. 113*, 4371−4380.
69. Tjandra, N., Feller, S. E., Pastor, R. W., and Bax, A. (1995) *J. Am. Chem. Soc. 117*, 12562−12566.
70. Hiyama, Y., Niu, C.-H., Silverton, J. V., Bavoso, A., and Torchia, D. A. (1988) *J. Am. Chem. Soc. 110*, 2378−2383.
71. Fairbrother, W. J., Liu, J., Pisacane, P. I., Sliwkowski, M. X., and Palmer, A. G. (1998) *J. Mol. Biol. 279*, 1149−1161.
72. Fushman, D., Tjandra, N., and Cowburn, D. (1998) *J. Am. Chem. Soc. 120*, 10947−10952.
73. Evenas, J., Forsen, S., Malmendal, A., and Akke, M. (1999) *J. Mol. Biol. 289*, 603−617.
74. Fisher, H. F., and Singh, N. (1995) *Methods Enzymol. 259*, 194−221.
75. Eftink, M. R., Anusiem, A. C., and Biltonen, R. L. (1983) *Biochemistry 22*, 3884−3896.
76. Horn, J. R., Russell, D., Lewis, E. A., and Murphy, K. P. (2001) *Biochemistry 40*, 1774−8.
77. Marion, D., Driscoll, P. C., Kay, L. E., Wingfield, P. T., Bax, A., Gronenborn, A. M., and Clore, G. M. (1989) *Biochemistry 28*, 6150−6156.
78. Marion, D., Kay, L. E., Sparks, S. W., Torchia, D. A., and Bax, A. (1989) *J. Am. Chem. Soc. 111*, 1515−1517.
79. Zuiderweg, E., and Fesik, S. (1989) *Biochemistry 28*, 2387−2391.
80. Russo, N., Shapiro, R., and Vallee, B. L. (1997) *Biochem. Biophys. Res. Commun. 231*, 671−674.
81. Leon-Lai, C. H., Gresser, M. J., and Tracey, A. S. (1996) *Can. J. Chem. 74*, 38−48.
82. Messmore, J. M., and Raines, R. T. (2000) *J. Am. Chem. Soc. 122*, 9911−9916.
83. Dwek, R. A. (1973) *NMR in Biochemistry: Applications to Enzyme Systems*, Clarendon Press, Oxford.
84. Millet, O. M., Loria, J. P., Kroenke, C. D., Pons, M., and Palmer, A. G. (2000) *J. Am. Chem. Soc. 122*, 2867−2877.
85. Loria, J. P., Rance, M., and Palmer, A. G. (1999) *J. Am. Chem. Soc. 121*, 2331−2332.
86. Borah, B., Chen, C., Egan, W., Miller, M., Wlodawer, A., and Cohen, J. S. (1985) *Biochemistry 24*, 2058−2067.
87. Palmer, A. G. (1993) *Curr. Opin. Biotechnol. 4*, 385−391.
88. Stivers, J. T., Abeygunawardana, C., and Mildvan, A. S. (1996) *Biochemistry 35*, 16036−16047.
89. Spolar, R. S., and Record, M. T. (1994) *Science 263*, 777−784.
90. Devore, J. (2000) *Probability and Statistics for Engineering and the Sciences*, Brooks/Cole Publishing Company, Monterey.
91. Dubins, D. N., Filfil, R., Macgregor, R. B., and Chalikian, T. V. (2000) *J. Phys. Chem. B 104*, 390−401.
92. Makhatadze, G. I., and Privalov, P. L. (1995) *Adv. Protein Chem. 47*, 307−425.
93. Privalov, P. L., and Makhatadze, G. I. (1993) *J. Mol. Biol. 232*, 660−679.
94. Pickett, S. D., and Sternberg, M. J. E. (1993) *J. Mol. Biol. 231*, 825−839.
95. Creamer, T. P., and Rose, G. D. (1992) *Proc. Natl. Acad. Sci. U.S.A. 89*, 5937−5941.
96. Prompers, J. J., and Bruschweiler, R. (2000) *J. Phys. Chem. 104*, 11416−11424.
97. Grzesiek, S., Stahl, S. J., Wingfield, P. T., and Bax, A. (1996) *Biochemistry 35*, 10256−10261.

BI034027H